






Article

On the Behavior of a Non-Linear Bandpass Filter with Self Voltage-Controlled Resistors

Ahmed S. Elwakil ^{1,2,3,*} , Mohamed B. Elamien ⁴ , Anis Allagui ⁵ , Brent J. Maundy ³ 
and Costas Psychalinos ⁶ 

¹ Department of Electrical and Computer Engineering, University of Sharjah, Sharjah P.O. Box 27272, United Arab Emirates

² Nanoelectronics Integrated Systems Center (NISC), Nile University, Giza 12677, Egypt

³ Department of Electrical and Software Engineering, University of Calgary, Calgary, AB T2N 1N4, Canada; bmaundy@ucalgary.ca

⁴ Department of Electrical and Computer Engineering, McMaster University, Hamilton, ON L8S 4L8, Canada; elamienm@mcmaster.ca

⁵ Department of Sustainable and Renewable Energy Engineering, University of Sharjah, Sharjah P.O. Box 27272, United Arab Emirates; aallagui@sharjah.ac.ae

⁶ Department of Physics, Electronics Laboratory, University of Patras, GR-26504 Rio Patras, Greece; cpsychal@upatras.gr

* Correspondence: elwakil@ieee.org

Abstract: In this work, we explore the behavior of a classical RLC resonance-based bandpass filter, which includes two resistors (one of which is associated with a non-ideal inductor), when either of these resistors is self voltage-controlled. In particular, self-feedback control is achieved by using the voltage developed across the inductor or the capacitor to dynamically change the value of the controlled resistor. This results in a multiplication-type non-linearity, which transforms the linear filter into a non-linear filter described by a set of non-linear differential equations. When gradually increasing the strength of the non-linearity, a notch-like behavior is observed at twice the resonance frequency. However, the non-linear filter can lose its stability with excessive feedback. Simulations and experimental results are provided to support the theory.

Keywords: analog filters; non-linear filters; resonance filters; band-pass filters; voltage-controlled resistors



Citation: Elwakil, A.S.; Elamien, M.B.; Allagui, A.; Maundy, B.J.; Psychalinos, C. On the Behavior of a Non-Linear Bandpass Filter with Self Voltage-Controlled Resistors.

Electronics **2024**, *13*, 3434. <https://doi.org/10.3390/electronics13173434>

Academic Editor: Djuradj Budimir

Received: 13 July 2024

Revised: 24 August 2024

Accepted: 28 August 2024

Published: 29 August 2024



Copyright: © 2024 by the authors. Licensee MDPI, Basel, Switzerland. This article is an open access article distributed under the terms and conditions of the Creative Commons Attribution (CC BY) license (<https://creativecommons.org/licenses/by/4.0/>).

1. Introduction

The study of non-linear resonance is a fundamental topic in circuit theory due to its numerous applications [1–3]. Non-linear resonators are used to widen the bandwidth of wireless power transfer systems [4] and reduce their sensitivity to position mismatch [5] because they can have more than one peak power frequency and can also show hysteresis behavior [6,7]. Non-linear resonance networks have also been widely used to model oscillatory systems such as the Van der Pol and Duffing oscillators [8,9], among others. However, little attention has been given to the filtering behavior and applications of these networks, as briefly demonstrated in our recent work [10]. In general, non-linear analog filters are not widely used, although some work has demonstrated their value in noise suppression [11–14]. Non-linear analog filters should not be confused with analog filters realized using non-linear analog circuits such as Log-domain circuits [15].

It is important to recall that non-linear resonators have been playing an increasingly important role in advancing wireless power transfer technologies and maintaining high power transfer efficiency despite changes in environmental parameters, such as the distance between transmitter and receiver or their relative alignment. Traditional linear resonators often show strong sensitivity to these variations, with large associated losses in power transfer efficiency. By contrast, non-linear resonant circuits, like parity-time symmetric or

Duffing resonators, are quite robust and can intrinsically accommodate parameter variations. For example, in [16], a non-linear parity-time-symmetric circuit utilized in a wireless power transfer system shows that an operation window is quite wide, wherein efficiency remains close to unity without the need for frequency tuning or internal coupling parameters. The result is that such systems become highly valuable in dynamic environments, where the relative positioning of transmitter and receiver changes, like in wireless charging of moving vehicles or medical devices. Additionally, the non-linear Duffing-based resonators can be integrated into wireless power transfer systems to improve their operational bandwidth [17]. This type of non-linear resonator has the ability to maintain a wide bandwidth and attaining a similar amplitude level compared to linear resonators, without the associated frequency sensitivity.

It is thus concluded that non-linear circuits play an important role in compensating for problems created by frequency detuning in wireless power transfer systems. Detuning can result from system parameter variations, such as inductance or capacitance, which result in a loss in transmission efficiency. In particular, non-linear resonant circuits developed to counter the influence of such effects are mainly based on the Van der Pol equation. These circuits exhibit a broadened frequency response that allows them to maintain high output power even when the working frequency is far from the resonant frequency. These make them suitable for applications in which a fine control of the frequency is difficult to realize or in systems that go through different loads and environmental conditions [18,19].

It is important to recall that a large number of non-linear resonators are modeled in normalized form by the forced Liénard second-order differential equation [20]

$$\ddot{x} + f(x)\dot{x} + g(x) = f(t). \quad (1)$$

The classical linear resonance network is described by (1) with $f(x) = 1/Q_r$ and $g(x) = \omega_r^2 x$, where Q_r is the quality factor of the resonance network and ω_r is its resonance frequency.

In this work, we focus our attention on a classical RLC bandpass filter and use self feedback to induce non-linearity, resulting in a non-linear bandpass filter. In particular, the voltage v_L developed across the inductor or the voltage v_C across the capacitor are used to dynamically change the value of the two resistors in the filter structure. This yields four possible non-linear filters, as depicted in Figure 1. However, none of these non-linear filters can be described by (1) as opposed to the circuits in [10]. In the filter of Figure 1a, the value of the resistance r_L is controlled via the capacitor voltage v_C , whereas in Figure 1b the feedback control uses the inductor voltage v_L . In Figure 1c,d, it is resistance R that is feedback-controlled. We show that as the strength of the feedback control voltage increases (i.e., magnitude of the non-linear term increases), a notch-like behavior is observed in the magnitude response of the bandpass filter at twice the resonance frequency, and a second notch develops at three times the resonance frequency with further increase in non-linearity. This notch behavior appears due to the inter-modulation terms resulting from the multiplication non-linearity. The non-linear filter's quality factor, and hence its bandwidth, is also shown to be modulated by the non-linearity. However, these non-linear filters have a narrow stability range and are not always stable. Numerical simulations are used to study the filters and experimental results support the predicted theory.

The work is organized as follows: the circuit analysis is performed in Section 2, while design examples are given in Section 3 and the obtained experimental results confirm the finding of this work.

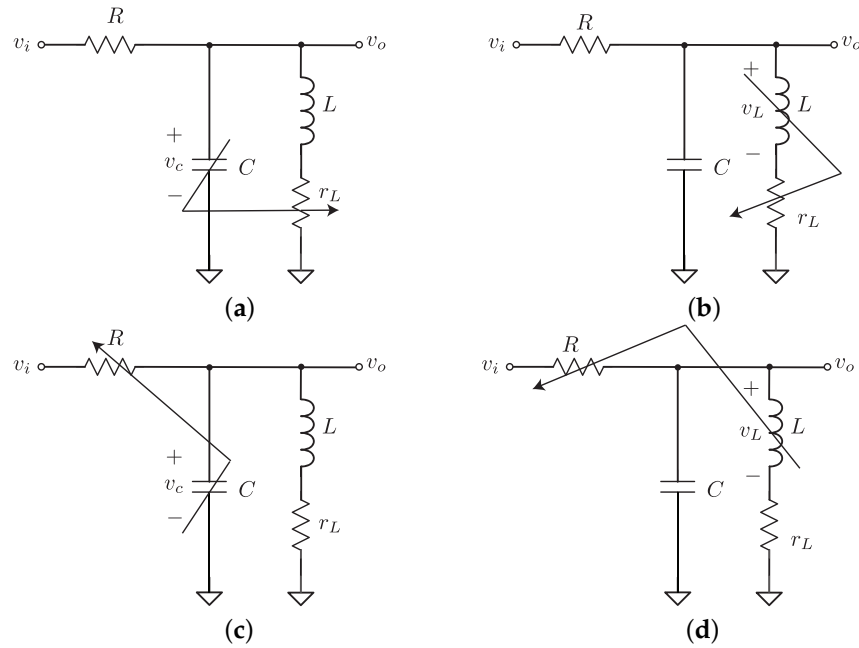


Figure 1. Classical bandpass filter based on parallel resonance when (a) r_L is controlled by v_C , (b) r_L is controlled by v_L , (c) R is controlled by v_C , and (d) R is controlled by v_L .

2. Circuit Analysis

Consider the circuit shown in Figure 1a, which is a classical bandpass filter based on a parallel LC resonance network. The transfer function of this filter is given by:

$$H_L(s) = \frac{Qs + \epsilon}{s^2 + (Q + \frac{\epsilon}{Q})s + (1 + \epsilon)} = \frac{1}{1 + \frac{s}{Q} + \frac{1}{Qs}} \Big|_{\epsilon=0}, \tag{2}$$

where we define $1/Q = R\sqrt{C/L}$ and $\epsilon = r_L/R$. This transfer function reduces to an ideal bandpass filter when the inductor is ideal and hence r_L tends to zero (i.e., $\epsilon \rightarrow 0$). Note that $s = j\omega_n$ in (2) is normalized with respect to the resonance frequency $\omega_r = 1/\sqrt{LC}$ ($\omega_n = \omega/\omega_r$), hence setting the filter’s ideal center frequency at $\omega_n = 1$.

2.1. Voltage-Controlled r_L

Now, let us consider that r_L is replaced with a physical resistance composed of a fixed part r_f and a voltage-controlled part r_v ; i.e.,

$$r_L = r_f \pm r_v \left(\frac{v_C}{v_{ref}} \right), \tag{3}$$

where v_C is the voltage on the capacitor and v_{ref} is an arbitrary reference voltage. This change in the circuit structure transforms the filter into a non-linear filter, which can be seen by writing the state-space model of the circuit (see Figure 1a):

$$C \frac{dv_C}{dt} = \frac{v_i - v_C}{R} - i_L, \quad L \frac{di_L}{dt} = v_C - i_L r_L, \tag{4}$$

where i_L is the inductor current. We introduce the dimensionless variables $x = v_C/v_{ref}$, $y = i_L R/v_{ref}$, $\epsilon_1 = r_f/R$, $\epsilon_2 = r_v/R$, transforming (4) into:

$$\frac{1}{Q} \dot{x} = -x - y + f(t) \tag{5}$$

$$Q\dot{y} = x - \epsilon_1 y \mp \epsilon_2 xy \tag{6}$$

where $f(t) = v_i/v_{ref}$ and time is normalized as $t = t \cdot \omega_n$. The non-linearity in (6) appears in the multiplication term $\epsilon_2 x \cdot y$, which will disappear only when $\epsilon_2 = 0$, i.e., r_L becomes a fixed resistance. Numerical simulation results of the above set of differential equations with $f(t) = A \sin \Omega t$ are plotted in Figure 2 for $Q = A = \Omega = 1, \epsilon_1 = 0.1$ and for four different values of ϵ_2 , namely $\epsilon_2 = (0, 0.1, 0.5, 1)$ (see first two columns of the figure). It is clear from these results that a stable limit cycle is observed in all cases, indicating that the filter remains stable despite the increasing strength of the non-linear term ϵ_2 . The filter remains stable until $\epsilon_2 \approx 2$, and beyond this value, the trajectories diverge.

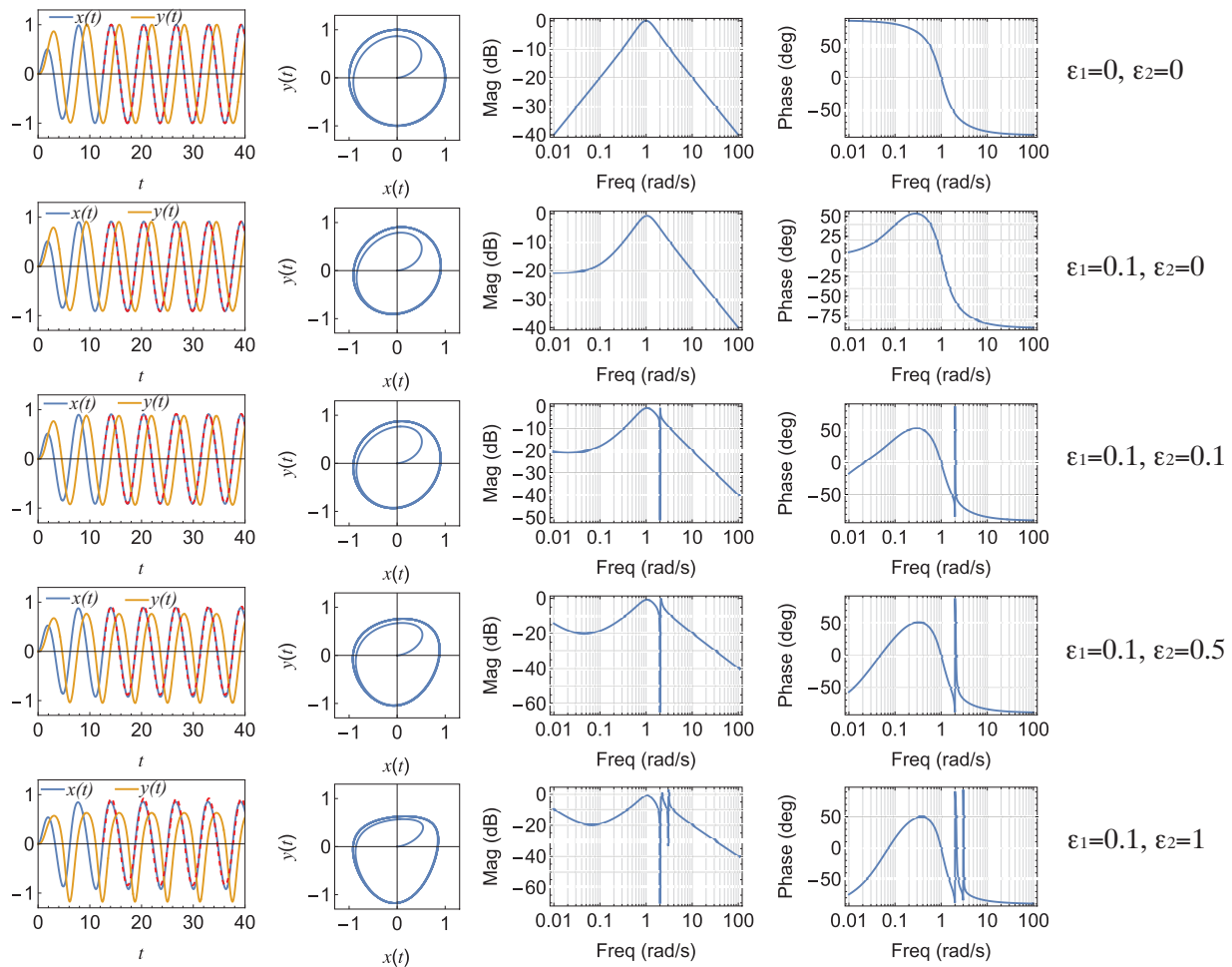


Figure 2. Numerically simulated time-domain waveforms of $x(t)$ and $y(t)$ obtained from (5) and (6) and corresponding magnitude and phase responses calculated using (7). First and second rows correspond to linear bandpass filter response and remaining rows correspond to non-linear filter response at increasing non-linearity strength. The best fit waveform of $x(t)$ is also plotted as a dashed red curve, compared to the exact waveform in blue.

The linear filter transfer function (2) can be retrieved only when $\epsilon_2 = 0$. When $\epsilon_2 \neq 0$, we obtain the following transfer function:

$$H_N^{-1}(s) = 1 + \frac{s}{Q} + \frac{1}{Qs + \epsilon_1} \mp \left(\frac{\epsilon_2}{Qs + \epsilon_1} \right) \left(\frac{\mathcal{L}x(t)y(t)}{X(s)} \right), \tag{7}$$

where $\mathcal{L}x(t)y(t)$ is the Laplace transform of the non-linear term. Note that (7) for $\epsilon_1 = 0$ (i.e., ideal inductor) can also be re-written as:

$$H_N^{-1}(s) = 1 + \frac{s}{Q} + \frac{1}{Q_N(s)s}, \tag{8}$$

where $Q_N(s) = Q/(1 \mp \epsilon_2 \frac{\mathcal{L}x(t)y(t)}{X(s)})$. When compared to the linear bandpass filter transfer function (2), it is clear that the non-linear term modulates the quality factor of the filter. To evaluate the magnitude and phase responses of (7), we perform the following steps:

- solve numerically the differential equations of the system for different values of ϵ_2 ;
- obtain the best fit expressions for $x(t), y(t)$, and hence compute $x(t) \cdot y(t)$;
- find $X(s)$ and $\mathcal{L}x(t)y(t)$ from the best fit expressions;
- use (7) to obtain the magnitude and phase responses of $H_N(s)$.

Following the above procedure, we show in Figure 2 (columns 3 and 4) plots of the filter’s magnitude and phase responses when $\epsilon_2 = (0, 0.1, 0.5, 1)$. We note that the ideal bandpass response with center frequency located at the normalized value $\omega_n = 1$ is observed. However, for higher values of ϵ_2 , a notch-like behavior appears at twice the normalized center frequency, i.e., at $\omega_n = 2$ when $\epsilon_2 = (0.1, 0.5)$ and then a second notch appears at $\omega_n = 3$ when $\epsilon_2 = 1$ (very strong non-linearity). Sharp changes can also be seen in the phase response at these critical frequencies. To verify this behavior further, an input signal $f(t) = \sin(\omega_n t) + \sin(2\omega_n t)$ was used with ω_n varied in the range (0.1 – 10). At each frequency, we isolated the first and second harmonics of $x(t)$, measuring their amplitudes. The results are plotted in Figure 3, where, consistently, we observed an attenuation in the amplitude of the second harmonic that intensifies with increasing ϵ_2 .

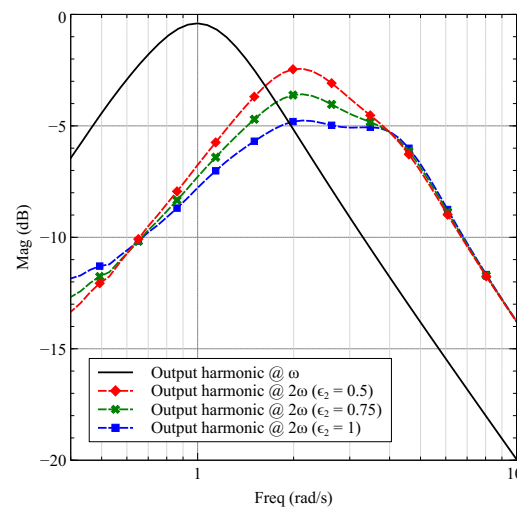


Figure 3. Numerical simulation results of (5) and (6) at $\epsilon_1 = 0.1$ and $\epsilon_2 = (0.5, 0.75, 1)$, showing the amplitude versus frequency of the first and second harmonics of $x(t)$ when the input signal is $f(t) = \sin(\omega_n t) + \sin(2\omega_n t)$, verifying the consistent attenuation at twice the resonance frequency.

In Table 1, the corresponding filter transfer functions $H_N(s)$ (obtained using (7)) in each case are provided. It is important to mention here that the magnitude and phase of $H_N(s)$ cannot be experimentally obtained using classical frequency-sweep analyzers. This is confirmed later in the experimental results section.

Now, consider the circuit shown in Figure 1b, where the inductor voltage v_L is used to control the resistor r_L (recall Equation (3)) instead of the capacitor voltage v_C . It can be shown that the circuit is hence described by the equations:

$$\frac{1}{Q}\dot{x} = -x - y + f(t), \quad Q\dot{y} = \frac{x - \epsilon_1 y}{1 \pm \epsilon_2 y}. \tag{9}$$

Numerical simulations of these differential equations with $f(t) = A \sin \Omega t$ are plotted in Figure 4 when $Q = A = \Omega = 1, \epsilon_1 = 0.1$ and for three different values of ϵ_2 , namely $\epsilon_2 = (0, 0.1, 0.5)$ (see first two columns of the figure). A stable limit cycle is observed, indicating that the filter is stable, until $\epsilon_2 \approx 0.65$, where the trajectories diverge and the filter becomes unstable. The stability range of this filter is therefore narrower than the one of Figure 1a, and its non-linear transfer-like function is given by

$$H_N^{-1}(s) = H_L^{-1}(s) \pm \left(\frac{\epsilon_2}{s + \epsilon_1/Q} \right) \left(\frac{\mathcal{L}y(t)\dot{y}(t)}{X(s)} \right). \tag{10}$$

Following a similar procedure to that described above, in Figure 4, a plot of the non-linear filter’s magnitude and phase responses compared to the linear filter’s response ($\epsilon_2 = 0$) is shown. Again, it is noted that a notch-like response appears at twice the normalized resonance frequency as ϵ_2 is increased with a corresponding change in the phase response.

Table 1. Transfer functions obtained using (7), corresponding to the magnitude and phase responses plotted in Figure 2 when $\epsilon_1 = 0.1$.

$\epsilon_2 =$	Transfer Function
0	$\frac{s+0.1}{s(s+1.1)+1.1}$
0.1	$\frac{(s+0.1) \left(\frac{0.91}{s^2+1} + \frac{0.004}{s} \right)}{(s(s+1.1)+1.1) \left(\frac{0.91}{s^2+1} + \frac{0.004}{s} \right) - 0.1 \left(\frac{0.041}{s} - \frac{0.82}{s^2+4} \right)}$
0.5	$\frac{(s+0.1) \left(\frac{0.90}{s^2+1} + \frac{0.019}{s} \right)}{(s(s+1.1)+1.1) \left(\frac{0.90}{s^2+1} + \frac{0.019}{s} \right) - 0.5 \left(\frac{0.041}{s} - \frac{0.79}{s^2+4} \right)}$
1	$\frac{(s+0.1) \left(\frac{0.88}{s^2+1} + \frac{0.04}{s} \right)}{(s(s+1.1)+1.1) \left(\frac{0.88}{s^2+1} + \frac{0.04}{s} \right) - \left(\frac{0.043}{s} - \frac{0.726}{s^2+4} \right)}$

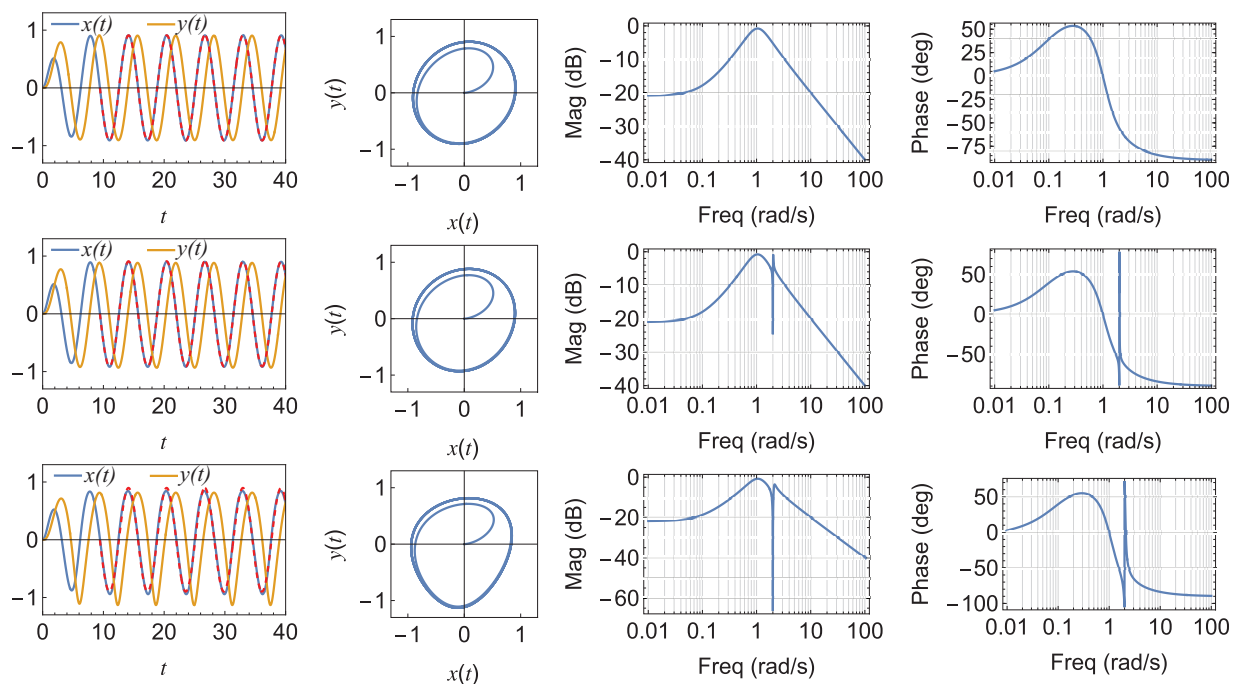


Figure 4. Numerical simulation results of (5) and (9) with corresponding magnitude and phase responses calculated using (10). First row corresponds to linear response at $\epsilon_1 = 0.1$ and $\epsilon_2 = 0$ and remaining rows correspond to non-linear filter response at $\epsilon_1 = 0.1$ and $\epsilon_2 = (0.1, 0.5)$, respectively. Best fit waveform of $x(t)$ is also plotted as a dashed red curve.

2.2. Voltage-Controlled R

Consider the circuit shown in Figure 1c, where v_C controls the resistor R , which is composed of a fixed part R_f and a variable part R_v such that:

$$R = R_f \pm R_v \left(\frac{v_C}{v_{ref}} \right). \tag{11}$$

Defining $x = v_C/v_{ref}$, $y = i_L r_L/v_{ref}$, $\epsilon_1 = R_f/r_L$, $\epsilon_2 = R_v/r_L$, and $1/Q = r_L\sqrt{C/L}$, it can be shown that this filter is described by the set of equations:

$$\frac{1}{Q}\dot{x} = \frac{f(t) - x}{\epsilon_1 \pm \epsilon_2 x} - y, Q\dot{y} = x - y. \tag{12}$$

where the non-linearity is clearly of the form $\epsilon_2 x \dot{x}$ and $\epsilon_2 x y$. Therefore, it is too complicated to proceed forward with computing the transfer function for this non-linear system.

Similarly, for the circuit in Figure 1d, where v_L controls resistor R , the describing equations are:

$$\frac{1}{Q}\dot{x} = \frac{f(t) - x}{\epsilon_1 \pm \epsilon_2(x - y)} - y, Q\dot{y} = x - y. \tag{13}$$

The non-linearity in this case is also complex. We investigated the stability of the above two filters numerically when $Q = A = \Omega = 1$, $\epsilon_1 = 0.1$ and found that both have a very limited stability range with respect to increasing ϵ_2 ($\epsilon_2 < 0.15$). Figure 5 shows the numerical simulations of (13) for $\epsilon_2 = (0, 0.1)$. The limited stability range can be improved at different values of Q , but this requires a more detailed study. In what follows, we focus our attention on the realization and experimental verification of the circuit in Figure 1a.

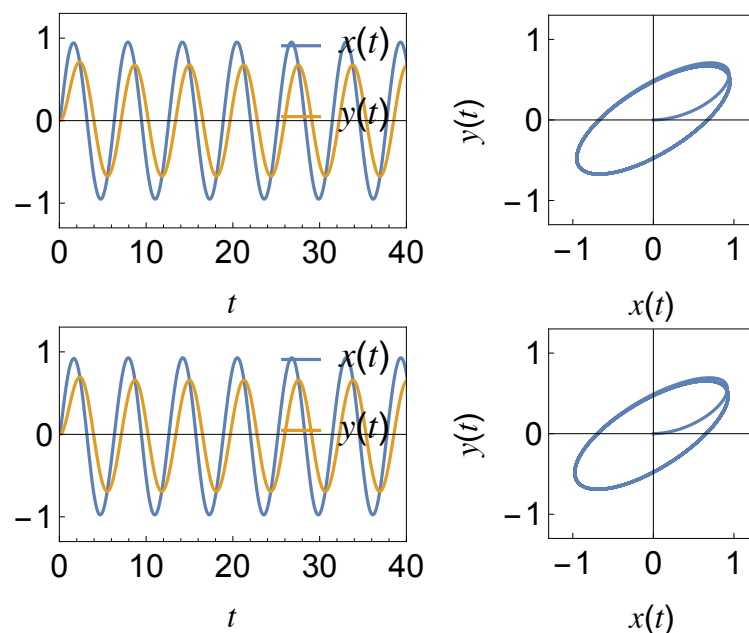


Figure 5. Numerical simulations of (12) for $\epsilon_1 = 0.1$ and $\epsilon_2 = (0, 0.1)$ demonstrating filter stability.

3. Circuit Design and Experimental Results

The non-linear bandpass filter in Figure 1a was realized using the circuit in Figure 6a. The resistor r_L in that circuit is composed of r_f in series with a MOSFET transistor, functioning as the variable resistor r_v . The voltage across the capacitor v_C is sensed by an operational amplifier, which subsequently controls the resistance of the MOSFET. The measurement results of this circuit were carried out with $L = 78$ mH (with a quality factor

of 20 at 10 kHz), $C = 3.2$ nF, and $R = 5$ k Ω . The LMC662 operational amplifier (powered by ± 5 V supplies) was used and was configured with $R_1 = R_2 = 100$ k Ω . An NMOS from a CD4007 transistor array was used and, for proper operation, a biasing circuit consisting of $C_b = 1$ nF, $R_b = 10$ k Ω and $V_b = 2.5$ V was used.

The measurement setup used for circuit validation is illustrated in Figure 6a. In the circuit of Figure 6b, r_f accounts for all fixed resistances, including a physical resistor of 100 Ω (needed to measure the inductor current), a parasitic resistor of 245 Ω associated with the non-ideal inductor and a fixed MOSFET resistance of 805 Ω . These circuit components and biasing voltage values correspond to a non-linear filter with $\epsilon_1 = 0.23$ and $\epsilon_2 = 0.15$. Figure 6c shows the experimentally measured waveforms of $x(t) = v_C(t)$ and $y(t) = i_L(t)R$ with an input signal of $v_{in}(t) = 0.5 \sin(2\pi 10^4 t)$.

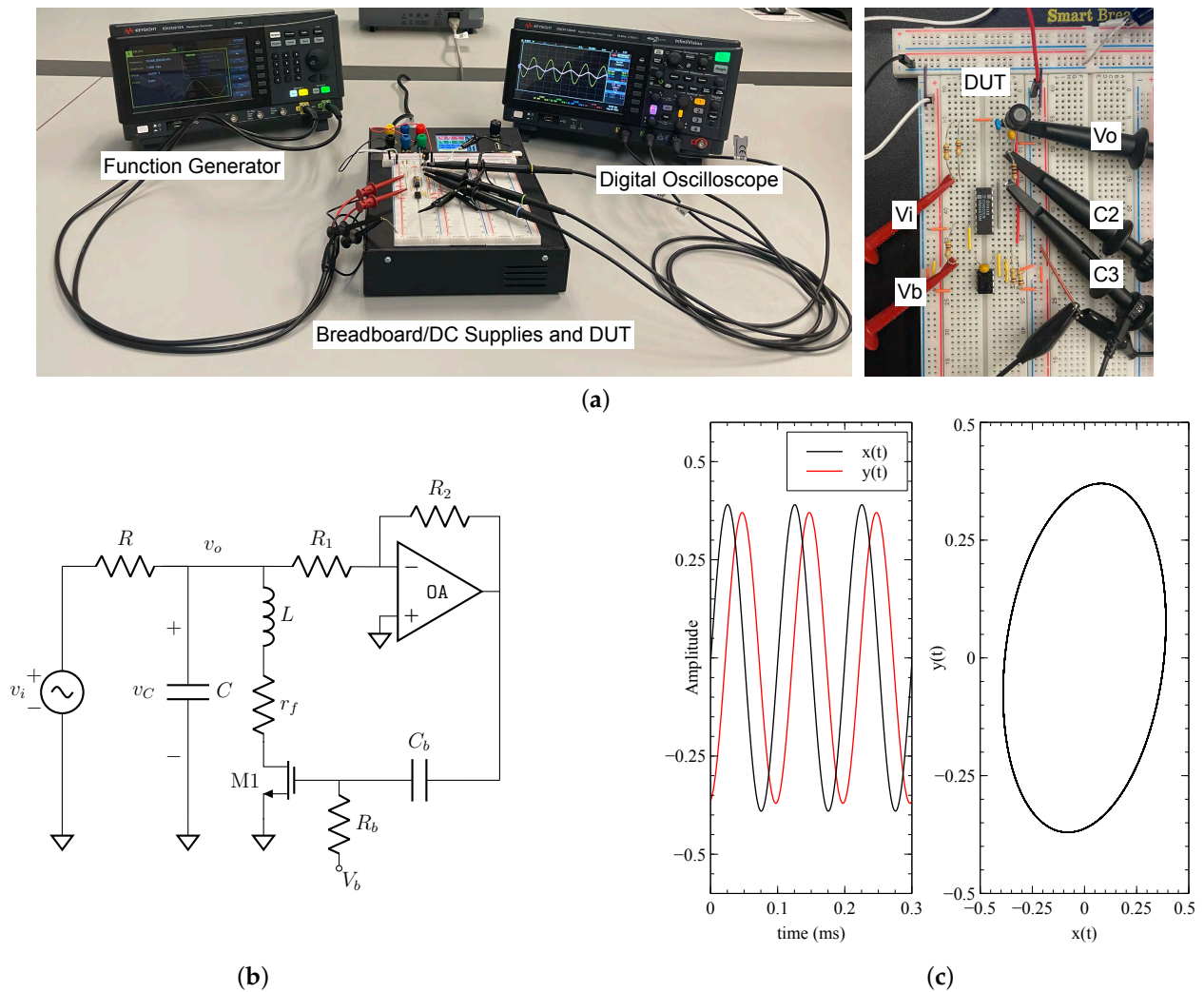


Figure 6. (a) Experimental setup for circuit validation, including signal source, measurement device, and power supply interfaced with the device under test (DUT). The oscilloscope channels (C₂ and C₃) are used to measured inductor current. (b) Schematic of the circuit implementation utilized for experimental measurements of the bandpass filter shown in Figure 1a. The resistance r_v is realized using a MOSFET, which is controlled by the voltage v_C . (c) Measured waveforms $x(t)$ and $y(t)$ corresponding to the non-linear filter response at $\epsilon_1 = 0.23$ and $\epsilon_2 = 0.15$.

Figure 7a shows the measured magnitude and phase responses of the circuit in Figure 6a. The transfer function $H(s)$ was directly obtained from data measured using a spectrum analyzer, while $H_N(s)$ was obtained by evaluating (7) with the measured waveforms of $x(t)$ and $y(t)$. This result shows a notch-like behavior around twice the

center frequency, as theoretically expected. The notch-like behavior was not captured by the spectrum analyzer, which employs a frequency sweeping method, because the transfer function (7) of the non-linear filter is dependent on both $X(s)$ and $\mathcal{L}x(t)y(t)$. Thus, the notch-like behavior can only be identified through post-processing the measured time-domain data of $x(t)$ and $y(t)$ or alternatively using a spectrum analyzer with a wide-band excitation signal rather than with frequency sweep. Figure 7b illustrates the bandwidth dependency of the non-linear filter on the input signal amplitude. Specifically, the 3-dB bandwidths were found to be 7.17 kHz, 7.30 kHz, and 7.43 kHz for input signal amplitudes of 1 V, 0.5 V, and 0.1 V, respectively. The filter bandwidth decreases with increased amplitude.

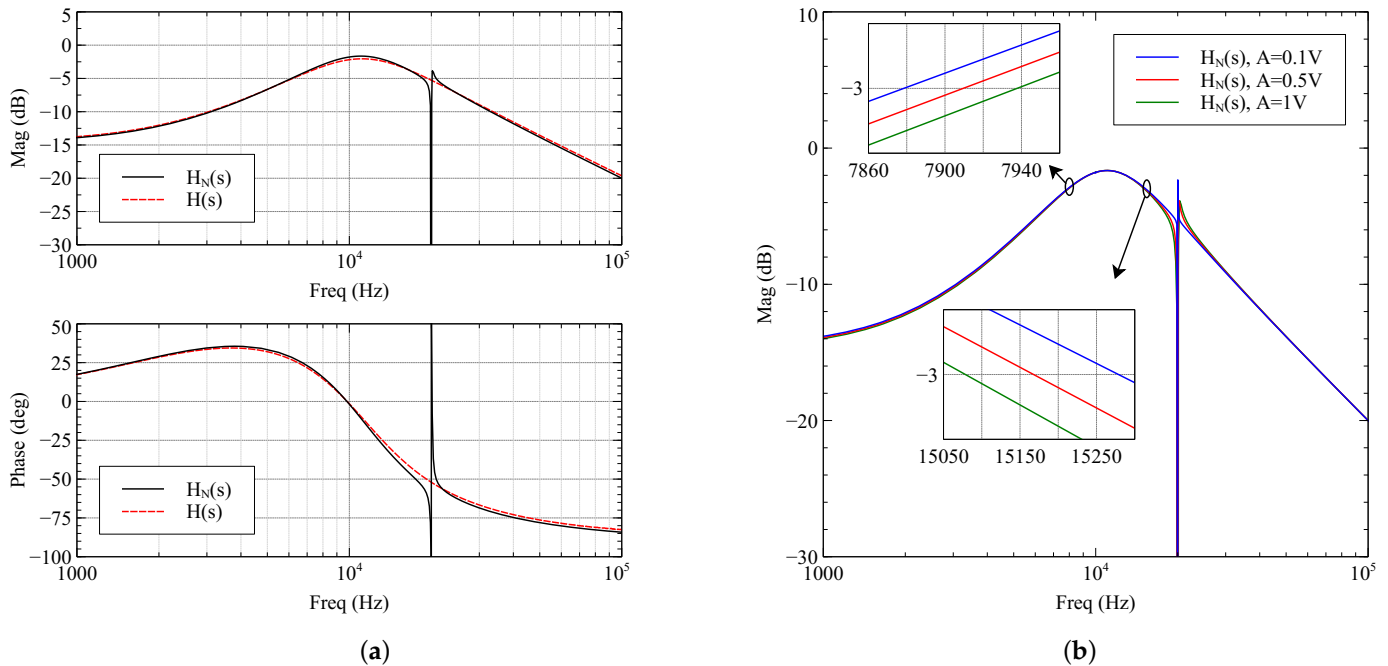


Figure 7. (a) Measured magnitude and phase responses of the circuit shown in Figure 6a at $\epsilon_1 = 0.23$ and $\epsilon_2 = 0.15$. $H(s)$ (represented by a dashed red line) is obtained directly from the spectrum analyzer, while $H_N(s)$ (shown as a solid black line) is obtained using (7) with the measured waveforms $x(t)$ and $y(t)$. (b) Measured magnitude responses at different input signal amplitudes $A = 0.1$ V, 0.5 V, 1 V.

The transfer functions in Table 1, which correspond to the cases of $\epsilon_1 = 0.1$ and $\epsilon_2 = 0, 0.5, 1$ were also implemented using the Field Programmable Analog Array (FPAA) AN231E04 device provided by Anadigm [21]. The clock frequency is equal to $f_{clk} = 250$ kHz. Using the *Anadigm Designer*® ver.2 software provided by Anadigm [21], the resulting design for implementing the transfer function for $\epsilon_2 = 0$ is depicted in Figure 8a, where the *FilterBiquad* Configurable Analog Modules (CAMs) have been employed. This originates from the fact that this biquadratic transfer function is decomposed as a sum of second-order band-pass and low-pass filter functions

$$H(s) = \frac{G_{BP1} \left(\frac{2\pi f_{01}}{Q} \right) s + G_{LP1} (2\pi f_0)^2}{s^2 + \frac{2\pi f_{01}}{Q_1} s + (2\pi f_{01})^2} \tag{14}$$

Employing the partial fraction expansion tool for decomposing the associated transfer functions that correspond to the cases of $\epsilon_2 = 0.5, 1$, the resulting simplified expression is

$$H(s) = \frac{G_{BP1} \left(\frac{2\pi f_{01}}{Q} \right) s + G_{LP1} (2\pi f_{01})^2}{s^2 + \frac{2\pi f_{01}}{Q_1} s + (2\pi f_{01})^2} + \frac{G_{BP2} \left(\frac{2\pi f_{02}}{Q_2} \right) s + G_{LP2} (2\pi f_{02})^2}{s^2 + \frac{2\pi f_{02}}{Q_2} s + (2\pi f_{02})^2} + \frac{G_{LP3} (2\pi f_{03})}{s + 2\pi f_{03}} \tag{15}$$

and the resulting design is demonstrated in Figure 8b, where the *FilterBiquad* and *Filter-LowFreqBilinear* CAMs are utilized.

Denormalizing the utilized transfer functions to the frequency 10 krad/s, the values of the characteristics of the filters, described by (14) and (15), are summarized in Table 2.

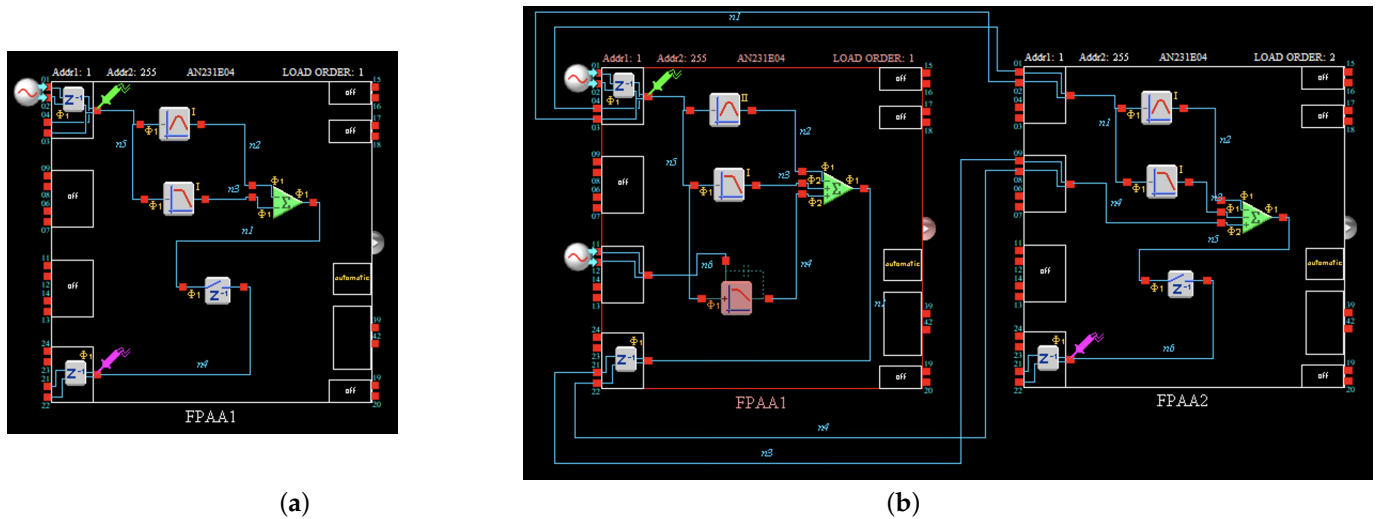


Figure 8. (a) FPAA-based implementation of the transfer function in (14) and (b) the associated implementation of the transfer function in (15).

Table 2. Values of the characteristics of the filters, described by (14) and (15).

Characteristic	$\epsilon_1 = 0.1$ and $\epsilon_2 = 0$	$\epsilon_1 = 0.1$ and $\epsilon_2 = 0.5$	$\epsilon_1 = 0.1$ and $\epsilon_2 = 1$
f_{01} (kHz)	10.49	20.78	21.58
Q_1	0.953	20.6	12.99
G_{BP1}	0.91	0.483	0.711
G_{LP1}	0.091	−0.042	−0.066
f_{02} (kHz)	—	10.68	10.78
Q_2	—	1.08	1.21
G_{BP2}	—	0.961	0.984
G_{LP2}	—	0.139	0.170
f_{03} (Hz)	—	3.66	8.39
G_{LP3}	—	4.65	3.89

The obtained input and output waveforms are demonstrated in Figures 9–11, while the measured values of the gain and phase at specific frequencies are summarized in Table 3. The corresponding theoretically predicted values are given between parentheses and confirm the accuracy of the presented implementations.

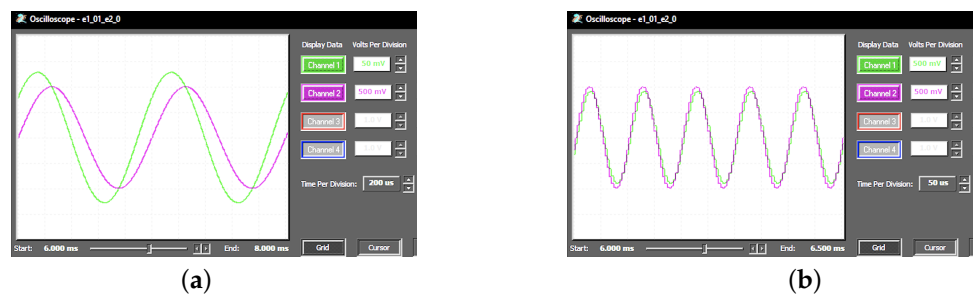


Figure 9. Input and output waveforms of the filter described by (14) for $\epsilon_1 = 0.1$ and $\epsilon_2 = 0$, stimulated by (a) 1 V, 1 kHz and (b) 1 V, 10 kHz sinusoidal signal.



Figure 10. Input and output waveforms of the filter described by (15) for $\epsilon_1 = 0.1$ and $\epsilon_2 = 0.5$, stimulated by (a) 1 V, 1 kHz and (b) 1 V, 10 kHz sinusoidal signal.



Figure 11. Input and output waveforms of the filter described by (15) for $\epsilon_1 = 0.1$ and $\epsilon_2 = 1$, stimulated by (a) 1 V, 1 kHz and (b) 1 V, 10 kHz sinusoidal signal.

Table 3. Values of the characteristics of the filters described by (14) and (15).

Characteristic	$\epsilon_1 = 0.1$ and $\epsilon_2 = 0$	$\epsilon_1 = 0.1$ and $\epsilon_2 = 0.5$	$\epsilon_1 = 0.1$ and $\epsilon_2 = 1$
gain at 1 kHz (dB)	-17.9 (-17.7)	-18.8 (-18.5)	(-18.7)
phase at 1 kHz ($^\circ$)	41 (39.2)	29 (28.2)	(16)
gain at 10 kHz (dB)	-0.9 (-0.8)	-0.9 (-0.8)	(-0.8)
phase at 10 kHz ($^\circ$)	0 (0)	0 (0)	(0)

4. Conclusions

In this study, we explored the dynamics of a non-linear RLC resonance-based bandpass filter with self-voltage-controlled resistors. Our investigations show that the non-linearity modulates the quality factor of the filter, and hence its bandwidth, but does not change the resonance frequency. The bandwidth is thus a function of the strength of the feedback signal and is dependent on the input signal amplitude. Also, a pronounced notch-like behavior appears at twice the resonance frequency. The technique presented here for transforming a linear filter into a non-linear one is not limited to the studied prototype example in Figure 1 and can be easily extended to other types of filters. Our future work will target transforming other passive and active filters from linear to non-linear filters using a similar self feedback control technique while examining the effects of this transformation on the filter parameters. It is needless to say that such a study cannot be automated and may or may not lead to identical findings, since the transformed filters are described by non-linear differential equations, which need to be solved numerically. It is also possible to use current-controlled resistors instead of voltage-controlled ones to obtain the non-linear filters.

Author Contributions: Conceptualization, A.S.E.; software, C.P., M.B.E. and B.J.M.; validation, C.P., M.B.E., A.A. and B.J.M.; formal analysis, A.S.E. and A.A.; investigation, C.P., M.B.E. and B.J.M.; writing—original draft preparation, A.S.E. and M.B.E.; writing—review and editing, C.P., A.A. and B.J.M. All authors have read and agreed to the published version of the manuscript.

Funding: This work was partially supported by the Natural Sciences and Engineering Research Council (NSERC) of Canada under its Discovery Grant (DG) program (RGPIN-2024-06826).

Data Availability Statement: The original contributions presented in the study are included in the article; further inquiries can be directed to the corresponding author.

Conflicts of Interest: The authors declare no conflicts of interest.

References

1. Ikehashi, T.; Maekoba, H.; Parent, A. Characterization of Nonlinear Behavior of Weakly Coupled Resonators Based on Nonlinearity Factor. *IEEE Sens. J.* **2021**, *21*, 24226–24237. [CrossRef]
2. Ardila, V.; Ramírez, F.; Suárez, A. Analytical and Numerical Bifurcation Analysis of Circuits Based on Nonlinear Resonators. *IEEE Trans. Microw. Theory Tech.* **2021**, *69*, 4392–4405. [CrossRef]
3. Coccolo, M.; Cantisan, J.; Seoane, J.M.; Rajasekar, S.; Sanjuan, M.A. Delay-induced resonance suppresses damping-induced unpredictability. *Philos. Trans. R. Soc. Math. Phys. Eng. Sci.* **2021**, *379*, 20200232. [CrossRef] [PubMed]
4. Yang, X.; Jiao, C.; Yang, J.; Fan, J.; Li, D.; Wang, B. Bandwidth Enhancement for Wireless Power Transfer System Employing Non-Linear Resonator. *IEEE Access* **2021**, *9*, 485–496. [CrossRef]
5. Abdelatty, O.; Wang, X.; Mortazawi, A. Position-Insensitive Wireless Power Transfer Based on Nonlinear Resonant Circuits. *IEEE Trans. Microw. Theory Tech.* **2019**, *67*, 3844–3855. [CrossRef]
6. Buscarino, A.; Famoso, C.; Fortuna, L.; Spina, G.L. Nonlinear Jump Resonance: Recent Trends From Analysis to Electronic Circuits Implementations. *IEEE Trans. Circuits Syst. II Express Briefs* **2024**, *71*, 1727–1732. [CrossRef]
7. Bucolo, M.; Buscarino, A.; Fortuna, L.; Frasca, M. Multiple Hysteresis Jump Resonance in a Class of Forced Nonlinear Circuits and Systems. *Int. J. Bifurc. Chaos* **2020**, *30*, 2050258. [CrossRef]
8. Chen, K.Y.; Biernacki, P.; Lahrichi, A.; Mickelson, A. Analysis of an experimental technique for determining Van der Pol parameters of a transistor oscillator. *IEEE Trans. Microw. Theory Tech.* **1998**, *46*, 914–922. [CrossRef]
9. Menzel, K.O.; Bockwoldt, T.; Arp, O.; Piel, A. Modeling Dust-Density Wave Fields as a System of Coupled Van der Pol Oscillators. *IEEE Trans. Plasma Sci.* **2013**, *41*, 735–739. [CrossRef]
10. Elwakil, A.S.; Allagui, A.; Psychalinos, C.; Maundy, B.J. A New Class of Nonlinear Resonance Networks Modeled by Levinson–Smith and Liénard Equations. *IEEE Trans. Circuits Syst. II Express Briefs* **2023**, *70*, 3669–3673. [CrossRef]
11. Barazideh, R.; Natarajan, B.; Nikitin, A.V.; Niknam, S. Performance Analysis of Analog Intermittently Nonlinear Filter in the Presence of Impulsive Noise. *IEEE Trans. Veh. Technol.* **2019**, *68*, 3565–3573. [CrossRef]
12. Barazideh, R.; Natarajan, B.; Nikitin, A.V.; Davidchack, R.L. Performance of analog nonlinear filtering for impulsive noise mitigation in OFDM-based PLC systems. In Proceedings of the 2017 IEEE 9th Latin-American Conference on Communications (LATINCOM), Guatemala City, Guatemala, 8–10 November 2017; pp. 1–6. [CrossRef]
13. Nikitin, A.V.; Scutti, D.; Natarajan, B.; Davidchack, R.L. Blind adaptive analog nonlinear filters for noise mitigation in powerline communication systems. In Proceedings of the 2015 IEEE International Symposium on Power Line Communications and Its Applications (ISPLC), Austin, TX, USA, 29 March–1 April 2015; pp. 1–6. [CrossRef]
14. Barazideh, R.; Nikitin, A.V.; Natarajan, B. Practical Implementation of Adaptive Analog Nonlinear Filtering for Impulsive Noise Mitigation. In Proceedings of the 2018 IEEE International Conference on Communications (ICC), Kansas City, MO, USA, 20–24 May 2018; pp. 1–7. [CrossRef]
15. Kontogiannopoulos, N.; Psychalinos, C. Switched-Current Filters Revisited: Square-Root Domain Sampled-Data Filters. *IEEE Trans. Circuits Syst. II Express Briefs* **2006**, *53*, 1373–1377. [CrossRef]
16. Assawaworrarit, S.; Yu, X.; Fan, S. Robust wireless power transfer using a nonlinear parity–time–symmetric circuit. *Nature* **2017**, *546*, 387–390. [CrossRef] [PubMed]
17. Wang, X.; Mortazawi, A. Bandwidth Enhancement of RF Resonators Using Duffing Nonlinear Resonance for Wireless Power Applications. *IEEE Trans. Microw. Theory Tech.* **2016**, *64*, 3695–3702. [CrossRef]
18. Wang, M.; Song, G.; Shi, Y.; Yin, R. Enhancement of robustness to frequency detuning with wireless power transfer based on Van der Pol resonance. *Int. J. Circuit Theory Appl.* **2022**, *50*, 4294–4306. [CrossRef]
19. Zhou, J.; Zhang, B.; Xiao, W.; Qiu, D.; Chen, Y. Nonlinear Parity-Time-Symmetric Model for Constant Efficiency Wireless Power Transfer: Application to a Drone-in-Flight Wireless Charging Platform. *IEEE Trans. Ind. Electron.* **2019**, *66*, 4097–4107. [CrossRef]
20. Wax, N. On Some Periodic Solutions of the Lienard Equation. *IEEE Trans. Circuit Theory* **1966**, *13*, 419–423. [CrossRef]
21. Anadigm. AN231E04 dpASP: The AN231E04 dpASP Dynamically Reconfigurable Analog Signal Processor. Available online: <https://anadigm.com/an231e04.asp> (accessed on 12 July 2024).

Disclaimer/Publisher’s Note: The statements, opinions and data contained in all publications are solely those of the individual author(s) and contributor(s) and not of MDPI and/or the editor(s). MDPI and/or the editor(s) disclaim responsibility for any injury to people or property resulting from any ideas, methods, instructions or products referred to in the content.